

# Clustering Left-Censored Multivariate Time-Series

Irene Y. Chen<sup>\*†</sup>, Rahul G. Krishnan<sup>‡</sup>, David Sontag<sup>†</sup>

## Abstract

Unsupervised learning seeks to uncover patterns in data. However, different kinds of noise may impede the discovery of useful substructure from real-world time-series data. In this work, we focus on mitigating the interference of left-censorship in the task of clustering. We provide conditions under which clusters and left-censorship may be identified; motivated by this result, we develop a deep generative, continuous-time model of time-series data that clusters while correcting for censorship time. We demonstrate accurate, stable, and interpretable results on synthetic data that outperform several benchmarks. To showcase the utility of our framework on real-world problems, we study how left-censorship can adversely affect the task of disease phenotyping, resulting in the often incorrect assumption that longitudinal patient data are aligned by disease stage. In reality, patients at the time of diagnosis are at different stages of the disease — both late and early due to differences in when patients seek medical care and such discrepancy can confound unsupervised learning algorithms. On two clinical datasets, our model corrects for this form of censorship and recovers known clinical subtypes.

## 1 Introduction

Cluster analysis of time-series data is a task of interest across a variety of scientific disciplines. Automating the discovery of latent patterns in such real-world data can be challenging due to the different patterns of noise in the data. Here, we focus on mitigating errata in the discovery of patterns due to left-censorship [1].

Left-censorship, in the context of time-series data, arises when time-series observations do not share a common starting point; consequently, common techniques for clustering can lead to erroneous conclusions about the underlying patterns therein. To address this, practitioners must often carefully and manually align data to a meaningful start time in order to find non-trivial clusters via unsupervised cluster analysis — a process whose difficulty can range from expensive and time-consuming in some problems to downright infeasible in others. In this work, we develop a machine learning algorithm that clusters time-series data while simultaneously correcting for potential left-censorship. In doing so, we can automate the time-consuming process of manual data alignment and use our method to reveal structure that would otherwise not be found by the straightforward application of clustering algorithms. The approach we propose is studied in the context of a variety of synthetic and real-world data but we ground the motivation for our model in a single example: disease phenotyping in healthcare.

Many diseases are biologically heterogeneous despite a common diagnosis—for example autism [2], heart failure [3], diabetes [4], and Parkinson’s disease [5]. The variation in biomarkers (e.g., glucose or creatinine) across patients can stem from different patient subtypes that manifest in distinct disease trajectories. Scientists

---

<sup>\*</sup>Corresponding author email: [iychen@mit.edu](mailto:iychen@mit.edu).

<sup>†</sup>Electrical Engineering and Computer Science, Massachusetts Institute of Technology, Cambridge, MA 02139, USA

<sup>‡</sup>Microsoft Research New England, Cambridge, MA 02139, USA

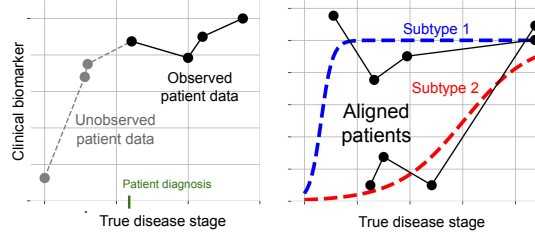


Figure 1: From censored longitudinal patient data aligned on first visit (**left**), we seek to understand disease heterogeneity by inferring subtypes after correcting for misalignment (**right**).

seek to understand this disease heterogeneity by identifying groups of people whose biomarkers behave similarly. For example, cardiologists use a measurement called ejection fraction as a heuristic to separate patients into two categories [6], but at least one of the two subtypes is believed to be heterogeneous [3]. To answer this question, cardiologists may turn to longitudinal, observational, and often irregularly-measured patient data.

Left-censorship in clinical datasets results when patients are aligned by first diagnosis or first hospital visit. Factors including geographic proximity to a hospital [7], financial access to care [8] or mistrust of the healthcare system [9] can affect when a patient seeks medical help and consequently the quality of their alignment with respect to the underlying progression of the diseases. For heart failure, a chronic disease that progresses over many years with a large range of onset ages and survival outcomes [10], these differences in patient alignment can confound attempts to analyse heterogeneity in the data. For a simplified illustration of the problem, see Figure 1 where the left figure depicts the common reality of observational health data and the right depicts the idealized latent substructure we would like to identify. Existing subtyping models applied to clinical data assume (potentially erroneously) that patients are aligned at the same point of disease stage. The problem with such an assumption is that the disparity between true disease stage and observed visit time can result in unsupervised learning algorithms uncovering the wrong, or perhaps less interesting, structure.

We formalize this problem setup and study identifiability under a noiseless model, showing both the degree of left-censorship and subtype labels are recoverable under reasonable model assumptions. Motivated by this result, we introduce a deep generative model for noisy data. Our approach—called SubLign—has the following properties:

1. SubLign makes no assumption on the distribution of alignment values beyond specifying extrema
2. SubLign operates on time-series with varying lengths and missing values, both characteristics often found in real-world datasets
3. SubLign is unsupervised, meaning that neither subtype labels nor alignment values are provided during training, and are only used in evaluation

We show robust quantitative results on synthetic data where, over multiple trials, our method outperform baselines for subtyping and patient alignment. We apply SubLign to two real-world clinical datasets—heart failure and Parkinson’s disease—and automatically recover known clinical subtypes without manual-alignment or expert knowledge.

## 2 Related Work

Learning alignment and clustering has been studied in fields across computer vision, signal processing, and health. Approaches often make assumptions including few discrete time steps [11, 12]; a single piecewise linear [11] or Gaussian mixture model [12] functional form; significantly more samples per object than number of objects [13, 14]; very small windows of potential misalignment [15, 16]; or known lag time [17]. Our method aims to cluster left-censored multivariate time series without these constraints.

Clinicians and scientists learn disease subtypes to better understand heterogeneity in disease progression in process known as *disease phenotyping*. Existing approaches often rely on the assumption that the observed measurements are aligned — and therefore not censored. Researchers then apply clustering techniques like hierarchical clustering of time series [2], affinity clustering [18], or matrix factorization [4, 19]. Other models define disease subtypes as stages of disease progression [20] instead. For this work, we define disease subtypes as separate from disease stage and jointly learn both.

## 3 Problem Setup and Identifiability

We observe data corresponding to  $N$  multivariate time-series, each of length up to  $M$ :

$$\begin{aligned} & \{[(x_{1,1}, y_{1,1}), \dots, (x_{1,M}, y_{1,M})], \\ & [(x_{2,1}, y_{2,1}), \dots, (x_{2,M}, y_{2,M})], \\ & \dots [(x_{N,1}, y_{N,1}), \dots, (x_{N,M}, y_{N,M})]\} \end{aligned} \quad (1)$$

where  $y_{i,m} \in \mathbb{R}^D$  is a vector of observations for time-series  $i$  at time-stamp  $x_{i,m} \in \mathbb{R}^+$ . We use  $Y_i = \{y_{i,1}, \dots, y_{i,M}\}$  and  $X_i = \{x_{i,1}, \dots, x_{i,M}\}$  to denote the collection of observations and time-stamps, respectively.

**Identifiability** We make no assumptions about the generative process of  $X_i$  other than distinct time stamps for  $M$  observations in  $X_i$ . We next describe the generative process for  $Y_i$ , which is conditional on  $X_i$ :

$$\begin{aligned} & \forall i = \{1, \dots, N\}, \\ & s_i \sim \text{Cat}(K), \delta_i \sim \text{Unif}(0, \delta^+), \\ & \forall m \in \{1, \dots, M\}, d \in \{1, \dots, D\} \\ & y_{i,m}[d] = f(\kappa(x_{i,m} + \delta_i; \theta^P[s_i, d])) \end{aligned} \quad (2)$$

$s_i \in \{1, \dots, K\}$  is the subtype for time-series  $i$  and  $\delta_i$  is the left-censored starting time. The link function  $f : \mathbb{R} \rightarrow \mathbb{R}$  has no parameters whereas  $\kappa : \mathbb{R} \rightarrow \mathbb{R}$  is an unknown polynomial function of degree  $P \in \mathbb{Z}^+$ . We denote the parameters of  $\kappa$ , for each subtype and dimension (biomarker), as  $\theta^P \in \mathbb{R}^{K \times D \times (P+1)}$ .  $\delta^+$  is the maximum alignment deviation. We denote  $\theta^P[s_i, d]$  as selecting the  $s_i, d$ -th index from the tensor  $\theta^P$ . Similarly,  $\theta^P[s_i]$  selects the  $s_i$ -th index. We define  $\theta_p$  as the  $p$ -th coefficient of any polynomial function parameter set  $\theta$ .

Note that, by construction,  $s_i = s_{i'} \iff \theta^P[s_i] = \theta^P[s_{i'}]$ , i.e., for two subtypes, each object's data is described either by  $y = f(\kappa(x; \theta))$  or  $y = f(\kappa(x; \theta'))$ .

We begin with a set of assumptions for identifiability.

**Assumption 1.**  $f$  is invertible, and  $\kappa(x, \theta) = \theta_0 + \sum_{p=1}^P \theta_p x^p$  describes a family of polynomial functions in  $x$  with parameter  $\theta$  and degree  $P > 0$  where each subtype has a distinct polynomial. The parameters of each subtype are unique.

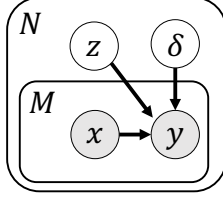


Figure 2: Graphical model of SubLign.

**Assumption 2.**  $M \geq P + 1$ , i.e., for each object, across all the  $J$  features, we observe at least  $P + 1$  values.

**Assumption 3.** For each subtype  $s_k$ , there exists an object  $i$  whose alignment  $\delta_i = 0$ .

**Theorem 1.** Under assumptions 1, 2, 3 for the model in Equation 2, we can identify the time-delays  $\delta_1, \dots, \delta_N$ . We can identify the polynomial coefficients  $\theta^P$  up-to a permutation of its rows and columns and the identity of  $s_1, \dots, s_N$  up-to a permutation over  $K$  choices.

We defer the proof for Theorem 1 to Appendix B. The proof is constructive: we describe a sequence of procedures, the first of which identifies the alignments for each patient and then uses the alignment and polynomial regression to identify the model parameters in Equation 1.

It is possible to relax Assumption 3 to only require the existence of one object from each subtype; however, this modification only allows identifiability of the values of censorship  $\delta_1, \dots, \delta_N$  up to a translation within each subtype.

## 4 SubLign: SUBtype & aLIGN

Theorem 1 describes conditions under which left-censorship and the polynomial parameters of cluster biomarker progression are identifiable. This encouraging result demonstrates scenarios where one can provably answer this challenging question from data. However, the model in Equation 2 has limitations including its inability to account for observational noise over time. The model we propose, SubLign, is a more practical approximation to the idealized model that jointly learns subtype and alignment from noisy data.

There are two stages to SubLign. In the first stage, we learn a model from the observed data, which disentangles variation in the observed data due to delays with variation related to subtype identity. In the next stage, we infer subtype representations for data and optionally cluster the representations to obtain the explicit subtype identity for each datapoint.

**SubLign Generative Model** We describe the latent-variable generative model of continuous-time data for SubLign. The graphical model is shown in Figure 2.

$$\begin{aligned}
 \forall i &= \{1, \dots, N\}, \forall j \in \{1, \dots, M\}, \forall d \in \{1, \dots, D\} \\
 \delta_i &\sim \text{Cat}(\mathcal{D}), z_i \sim \mathcal{N}(\mathbf{0}, \mathbf{I}), \Theta = g(z_i; \gamma), \\
 \hat{y}_{i,m}[d] &= f(\kappa(x_{i,m} + \delta_i; \Theta[d])), y_{i,m} \sim \mathcal{N}(\hat{y}_{i,m}, \mathbf{I}),
 \end{aligned} \tag{3}$$

Where relevant, for ease of exposition, we share notation between Equation 2 and Equation 3. For clarity, we will drop indices denoting patient identity and dimension when unnecessary. Random variable  $\delta_i \in \mathbb{R}^+$  indicates the degree of left-censorship associated with the set of patient biomarkers. We discretize the closed

interval  $[0, \delta^+]$  as  $\mathcal{D} = [0, \epsilon, 2\epsilon, \dots, \delta^+]$  with hyperparameter  $\epsilon$  and use a categorical distribution over  $\mathcal{D}$  with uniform probabilities over each element as our prior over  $\delta_i$ .

Rather than model subtype as a discrete latent variable, we opt to model disease heterogeneity of latent variation in the time-series via a continuous, low-dimensional random variable  $z_i \in \mathbb{R}^{N_z}$  with latent space dimension  $N_z$ .

Function  $g : \mathbb{R}^{N_z} \rightarrow \mathbb{R}^{D \times (P+1)}$  has parameters  $\gamma$  and maps from the latent variable to  $\Theta \in \mathbb{R}^{D \times (P+1)}$ , a matrix of parameters for  $D$  polynomials, each of degree  $P$ . As before,  $f$  is a known link function and describes how the observed values relate to the observed time-points.

**Parameterization** We discuss the specific parameterizations of Equation 3 that we study. In the context of the motivating application of disease phenotyping, these functions represent commonly found characteristics of the progression of patient biomarkers.

*Link function and polynomials:* For  $f$  and  $P$ , we study the following choices:

- *Sigmoid:*  $P = 1$  and  $f(x) = \frac{1}{1+\exp(-x)}$
- *Quadratic:*  $P = 2$  and  $f(x) = x$

The sigmoid function can represent bounded and monotonically increasing clinical variables. The quadratic can represent cases where biomarkers that denote severity decrease (likely in response to therapy) and then increase (once therapy fails), or vice versa. Other choices for  $P, f$  are permissible as long as they are differentiable with respect to the model parameters. We allow for the possibility that different biomarkers can have different parameterizations.

*Modeling polynomial parameters:* We parameterize  $g(z_i; \gamma)$  using a two layer neural network with ReLU activation functions with parameters  $\gamma$ . To be concrete, if  $D = 1, P = 2$ , and  $f$  is the sigmoid function, then the outputs of  $g$  are  $[\beta_0(z), \beta_1(z)]$  and  $y = \frac{1}{1+\exp(-(\beta_0(z)x + \beta_1(z)))}$ . Similarly, if  $D = 1, P = 1$ , and  $f$  is the quadratic function then the outputs of  $g$  are  $[a(z), b(z), c(z)]$  and  $y = a(z)x^2 + b(z)x + c(z)$ .

**Unpacking the SubLign model** We see that the latent variable  $z$  played an important role in quantifying how each biomarker behaves. Each time-series's latent variable is used to predict the parameters of  $D$  polynomial functions and  $f \circ \kappa$  maps from observed visit times onto the observed biomarkers. We will assume that time-series whose representation space  $z$  are *close*, hail from the same subtype and consequently manifest similar patterns in their biomarkers.

This notion of similarity is captured by the composition of  $f \circ \kappa$  since variation in  $z$  results in variation in the parameters  $\Theta$  and consequently in variation among the data as a function of the time-points. For example, when  $P = 1$  and  $f$  is the identity (i.e. we have a linear function), some time-series might increase (positive slope) versus others that decrease (negative slope). The latent representation  $z$  captures subtypes by learning to predict the slope of the function that models the variation among the time-series. Next, we describe the two stages of SubLign.

There are many routes to a practical model from Equation 2; the one we develop is a variant of a variational autoencoder [21] that makes use of recent advances in deep generative models to learn rich latent structures [22, 23] and advances in approximate inference to scale learning to larger datasets [24].

## 4.1 Learning

We learn the parameters  $\gamma$  of the model in Equation 3 via maximum likelihood estimation. Since the model is a non-linear latent variable model, we learn via maximizing the following variational lower bound on the

conditional likelihood of data given observation time-stamps (derived for a single patient’s sequence):

$$\begin{aligned}
& \log p(Y|X; \gamma) \\
&= \log \int_{Z, \delta} p(Y, Z, \delta|X; \gamma) dZ d\delta \\
&= \log \int_{Z, \delta} q(Z|X, Y; \phi) \frac{p(Y, Z, \delta|X; \gamma)}{q(Z|X, Y; \phi)} dZ d\delta \\
&\geq \int_{Z, \delta} q(Z|X, Y; \phi) \log \frac{p(Y, Z, \delta|X; \gamma)}{q(Z|X, Y; \phi)} dZ d\delta
\end{aligned} \tag{4}$$

We assume that the variational approximation for  $Z$  is parameterized via an inference network (with parameters  $\phi$ ), and the inequality in the above is by Jensen’s inequality. The lower bound can be rewritten as follows.

$$\begin{aligned}
\mathcal{L}(Y|X; \gamma, \phi) &= \mathbb{E}_{q(Z|X, Y; \phi)} \left[ \log \sum_{\delta} p(Y|X, \delta, Z; \gamma) p(\delta) \right. \\
&\quad \left. + \log \frac{p(Z)}{q(Z|X, Y; \phi)} \right]
\end{aligned} \tag{5}$$

Equation 5 is differentiable in  $\gamma, \phi$  using the re-parameterization [21, 24] trick for the outer expectation and the log-sum-exp trick for the inner sum. A natural next step would be to learn via gradient ascent on the objective function with  $\max_{\gamma, \phi} \sum_{i=1}^N \mathcal{L}(Y_i|X_i; \gamma, \phi)$ . However, we found this approach unstable, often getting stuck in poor local optima. Instead, we note that for all values of  $\hat{\delta}$ :

$$\begin{aligned}
\mathcal{L}(Y|X; \gamma, \phi) &> \mathcal{L}(Y|X; \gamma, \phi, \hat{\delta}) \\
&= \mathbb{E}_{q(Z|X, Y; \phi)} \left[ \log p(Y|X, \hat{\delta}, Z; \gamma) p(\hat{\delta}) \right. \\
&\quad \left. + \log \frac{p(Z)}{q(Z|X, Y; \phi)} \right]
\end{aligned} \tag{6}$$

Equation 6 could be an equality if all elements inside the sum over  $\delta$  in Equation 5 are the same. This, however, would imply that  $\delta$  has no effect on the conditional likelihood of the data, which is impossible by construction. We then learn via subgradient ascent as follows:

$$\max_{\gamma, \phi} \sum_{i=1}^N \max_{\delta \in \mathcal{D}} \mathcal{L}(Y_i|X_i; \gamma, \phi, \hat{\delta}_i) \tag{7}$$

where we obtain  $\hat{\delta}_i = \arg \max_{\delta \in \mathcal{D}} \mathcal{L}(Y_i|X_i; \gamma, \phi, \delta)$  and use this to derive gradients  $\nabla_{\gamma, \phi} \mathcal{L}(Y_i|X_i; \gamma, \phi, \hat{\delta}_i)$ .

The expectation in Equation 5 is identical to the variational lower bound used in learning variational autoencoders [21] and is amenable to gradient based learning via stochastic backpropagation. In practice, we use a recurrent neural network (RNN) to parameterize the inference network. We concatenate the observed visit times  $X$  and clinical biomarkers  $Y$  as inputs into the RNN with parameters  $\phi_1$ . We use the last hidden state of the RNN,  $h$ , to parameterize  $q(Z|X, Y) = \mathcal{N}(\mu(h; \phi_2), \Sigma(h; \phi_3))$  with  $\mu$  and  $\Sigma$  parameterized as neural networks with parameters  $\phi_2$  and  $\phi_3$ , respectively. The parameters of the inference network are the set  $\phi = \{\phi_1, \phi_2, \phi_3\}$ .

## 4.2 Obtaining Learned Subtypes

After learning the model, we may re-use the inference network to predict the latent variable  $z_i = \mu(h_i; \phi_2)$  for each patient in the training set. Combining  $z_i$  across all time-series gives us the set  $\mathcal{Z}$ . When reasonable, we refer to  $\mu(h_i; \phi_2)$  as  $\mu_i$ .

---

**Algorithm 1** SubLign

---

```
1: Input: Visit times  $X \in \mathbb{R}^{N \times M}$ , biomarkers  $Y \in \mathbb{R}^{N \times M \times D}$ 
2: Output:  $\tau_k$  for each subtype and  $\delta_i$  for each patient
3: Step 1: Learning
4: repeat
5:   Run RNN to obtain:  $h = \text{RNN}([X, Y])$ 
6:   Compute variational distribution  $q(Z|X, Y) = \mathcal{N}(\mu(h; \phi_2), \Sigma(h; \phi_3))$ 
7:   for patient  $i = 1$  to  $N$  do
8:     Run grid-search to find  $\delta_i$  that maximizes Equation 7
9:   end for
10:  Update  $\gamma, \phi$  using  $\nabla \mathcal{L}(Y|X; \gamma, \phi, \delta_i)$  as defined in Equation 5
11: until convergence
12: Step 2: Inference and Clustering
13: Infer  $\mathcal{Z} = \{z_i | z_i = \mu(h_i; \phi_2)\}$  for  $X_i, Y_i$ 
14: Find  $K$  clusters using K-Means on  $\mathcal{Z}$  and compute cluster centers  $\mu_k$ 
15: Learn subtype trajectories  $\tau_k = g(\mu_k)$ 
```

---

Although the latent variable  $z_i$  encodes latent structure from the patients, we may be interested in the explicit subtypes for a given value of  $K$ . To obtain discrete sub-types, we can run  $k$ -Means clustering on  $\mathcal{Z}$  to obtain the  $K$  cluster means  $\{\mu_1, \dots, \mu_K\}$ . We then compute  $\{\tau_1, \dots, \tau_K\}$  where  $\tau_i = g(\mu_i)$  as the progression-patterns corresponding to each of the discrete subtypes of the disease. For example, if  $f \circ \kappa$  is linear, then we obtain  $K$  different slopes and biases, each of which describes how the time-series behaves in that subtype. In practice,  $K$  may be chosen based on domain knowledge; alternatively, qualitative results can be assessed for each version of  $K$ , e.g. by plotting the corresponding  $f$  functions. We present SubLign using pseudocode in Algorithm 1.

## 5 Evaluation Setup

### 5.1 Datasets

**Synthetic data** We generate two classes of synthetic datasets from the *sigmoid* and *quadratic* parameterizations in Section 4. The former mimics situations where the patient’s condition steadily deteriorates. The latter mimics situations where the patient’s condition deteriorates and then improves through the course of the disease, or vice versa. For the sigmoid dataset, we generate data from  $K = 2$  subtypes and  $D = 3$  biomarker dimensions. For the quadratic dataset, we generate data with  $K = 2$  and  $D = 1$ . We provide the data generation process for the six quadratic datasets in the appendix. Each dimension is independent of other dimensions.

Each patient’s data are assumed to have been modulated depending on which of the two different subtypes they are drawn from. For the sigmoid dataset, the first subtype generating function across three dimensions is  $f_1(t) = [\sigma(-4+t), \sigma(-1+t), \sigma(-8+8t)]$  and the second subtype generating function is  $f_2(t) = [\sigma(-1+t), \sigma(-8+8t), \sigma(-25+3.5t)]$ . Note that although the first biomarker for both subtypes are shifted representations of each other, the second and third biomarkers allow identifiability. For each patient in both synthetic settings, we sample subtype  $s \sim \text{Bern}(0.5)$ . The true disease stage is drawn  $t_m \sim \text{Unif}(0, T^+)$  for visit  $m \in \{1, \dots, M\}$ . The biomarker values are drawn  $y_m \sim N(\lambda_m, \sigma^2)$  where  $\lambda_m = \sum_{k \in \{1, \dots, K\}} \mathbb{1}(s_i = k) f_k(t_m)$ . The observed disease time  $x_m$  is shifted such that the first patient visit is at time 0. Therefore  $x_m = t_m - \zeta$  where  $\zeta = \min_{j \in \{1, \dots, M\}} t_j$

is the earliest true disease time for the patient. We sample  $N = 1000$  patients with  $M = 4$  visits, variance  $\sigma^2 = 0.25$ , and max disease stage  $T^+ = 10$ .

**Real-world clinical data** We apply our algorithm to two real-world clinical datasets to assess its performance when data have realistic dynamics and are missing over time. We explain our handling of missing data in the appendix.

For heart failure (HF), we use electronic health records from a large health system in the United States. We identify patients who enter the emergency department with a diagnosis of HF and extract echocardiogram values—measurements from an ultrasound of the heart—from hospital visits before, during, and after the diagnosing emergency department visit. We include echo features that are present in more than 60% of echo studies. Our dataset includes  $N = 1534$  patients and  $D = 12$  features with  $M = 38$  maximum visits per patient. We extract 27 baseline features including race, sex, and comorbidities (e.g. renal failure) to validate subtypes. The dataset is aligned by first visit with transformed echo values between 0 and 1 with larger values denoting more abnormal values.

For Parkinson’s disease (PD), we use data from the Parkinson’s Progression Markers Initiative (PPMI), an observational clinical study, totalling  $N_t = 423$  PD patients and  $N_c = 196$  healthy controls where  $N = N_t + N_c$ . We extract four biomarker measurements of autonomic, motor, non-motor, and cognitive ability from  $N = 619$  total participants with  $M = 17$  maximum visits per patient. Our baseline data include 25 features including demographic information and patient history used to validate subtypes. The dataset is aligned by enrollment in the study (meaning PD diagnosis within the past two years), and measurements are scaled between 0 and 1 with larger values corresponding to more abnormal values. We use the sigmoid parameterization of the SubLign model for both datasets because HF and PD are chronic and incurable diseases.

## 5.2 Hyperparameters

We find optimal hyperparameters via grid search. For both synthetic and clinical experiments, we search over hyperparameters including dimensions of the latent space  $z$  (2, 5, 10), the number of hidden units in the RNN (50, 100, 200), the number of hidden units in the multi-layer perceptron (50, 100, 200), the learning rate (0.001, 0.01, 0.1, 1.), regularization parameter (0., 0.1, 1.), and regularization type (L1, L2). We select the hyperparameter configuration with the best validation loss, as measured by Equation 6. Our algorithms are implemented in Python 3.6, use the PyTorch autograd library [25], and optimize with Adam [26]. Our runtime is impacted by the grid search over  $\delta_i$ , which is a model parameter. We set alignment extrema  $\delta^+ = 5$  based on the maximum of the synthetic dataset and the maxima of the HF and PD datasets. We search over 50 alignment time steps (i.e.,  $\epsilon = 0.1$ ).

## 5.3 Baselines

We compare to eight different baselines. Our greedy baseline, denoted as KMeans+Loss, first clusters the observed values using  $k$ -means clustering. Then, using the inferred labels  $s$ , we simultaneously learn  $\theta_k$  for each subtype and  $\delta_i$  for each patient by minimizing:

$$\arg \min_{\theta, \delta} \sum_{i=1}^N \sum_{j=1}^M \sum_{d=1}^D \sum_{k=1}^K \mathbb{1}[s_i = k] [y_{i,j,d} - f(x_{i,j,d} + \delta_i; \theta_k)]^2 \quad (8)$$

using Broyden–Fletcher–Goldfarb–Shanno. This naive clustering based approach (in the space of the original data) attempts to correct for shifts in time. We also compare to:



1. SubNoLign, a modified SubLign with no alignment value. This is comparable to [27], which also leverages a deep latent representation, while implementing architectural choices similar to SubLign
2. SuStaIn [11], a subtype and stage inference algorithm for disease progression
3. A Bayesian approach [12] designed to consider longitudinal disease progression data without knowing the functional form of the data
4. PAGA [28], a state-of-the-art single-cell trajectory pseudo-time method
5. Dynamic time warping using kernel methods [29] and soft-DTW [30]
6. Tensor factorization phenotyping for sparse data [19]

For cross-sectional baselines (i.e., [11], [28]), we remove time information to convert from longitudinal to cross-sectional data. We detail other baseline implementations in the appendix.

## 5.4 Evaluation

We evaluate models and baselines on the same train, validation, and test data for each trial. For all metrics, we learn on a training set (60%), find the best performance across all hyperparameters on the validation set (20%), and report the best performance on the test set (20%).

We report the performance on the test set over three metrics. *Adjusted Rand index (ARI)* measures whether pairs of samples are correctly assigned in the same or different subtypes [31]. The *Swaps metric* reports the number of swaps needed to sort the predicted disease times into the true disease stages, expressed as percentage of total possible swaps, with full equation in the appendix. The *Pearson correlation coefficient* expresses correlation between the predicted and true disease stage. ARI measures the clustering performance while the Swaps metric and the Pearson correlation coefficient quantify how well the learning algorithm infers the alignment values.

Table 1: Sigmoid data experiment means and standard deviations over 5 trials with 1000 patients, 3 dimensions, and 4 visits per patient.

MODEL	ARI $\uparrow$	SWAPS $\downarrow$	PEARSON $\uparrow$
SubLign	<b><math>0.94 \pm 0.02</math></b>	<b><math>0.09 \pm 0.00</math></b>	<b><math>0.85 \pm 0.04</math></b>
SubNoLign	$0.81 \pm 0.21$	–	–
KMeans+Loss	$0.67 \pm 0.04$	$0.21 \pm 0.03$	$0.49 \pm 0.01$
SuStaIn [11]	$0.66 \pm 0.02$	$0.16 \pm 0.00$	$0.30 \pm 0.02$
Bayesian [12]	$0.19 \pm 0.18$	$0.48 \pm 0.00$	$0.01 \pm 0.02$
PAGA [28]	$0.32 \pm 0.05$	$0.52 \pm 0.07$	$0.04 \pm 0.20$
Soft-DTW KMeans [29]	$0.06 \pm 0.01$	–	–
Kernel KMeans [32]	$0.06 \pm 0.07$	–	–
Tensor Factorization [19]	$0.22 \pm 0.18$	–	–

**Quantitative metrics on clinical datasets:** Because real world data often lack ground truth labels for subtype or alignment, we create two semi-synthetic experiments for our clinical datasets. For HF, we evaluate SubLign’s ability to infer disease stage by modifying the test set and dropping visit observations. We train SubLign using 80% data (train and validation data) as normal. We modify the remaining data (20%) by

removing the first year of patient visits, creating distorted test set  $\{X', Y'\}$ , and by removing the last year of patient visits, creating  $\{X'', Y''\}$ . We compare the predicted alignment values  $\delta' = \text{SubLign}(X', Y')$  and  $\delta'' = \text{SubLign}(X'', Y'')$ . By construction, we expect  $\delta' > \delta''$ , and we measure the percentage of patients for which SubLign is able to recover this relationship.

For PD, because our dataset includes healthy control patients and patients with PD, we evaluate the held-out clustering performance using the disease status (PD patient or health control) as the  $K = 2$  labeled subtypes.

**Model misspecification:** Because our model implicitly assumes a functional form (e.g., sigmoid or quadratic), we investigate learning under model misspecification. We created synthetic datasets using splines on 5 randomly generated control points with the same noise rates, dimensions, and censoring as the original experiments. We create two settings: one where the control points are monotonically increasing and one with no restrictions. We run SubLign and use a sigmoid  $f$  function the monotonically increasing control points (labeled “Incr”) and use quadratic  $f$  function for splines generated without restrictions (labeled “Any”).

## 6 Evaluation and Analysis

Our evaluation addresses the following questions:

- How well does SubLign recover known subtypes in the presence of left-censorship?
- How well does SubLign recover alignment values?
- Are our discovered subtypes clinically meaningful?

### 6.1 Recovering Subtypes with Left-Censorship

**Sigmoid dataset** SubLign is able to recover subtypes despite left-censorship, outperforming all baselines (Table 1, ARI column). By clustering in the latent space of a deep generative model, SubLign can recover subtypes (mean ARI of 0.94) better than the KMeans+Loss baseline (0.67) which assumes a greedy approach. Not correcting for alignment time decreases the quality of inferred subtypes as can be seen in SubNoLign (0.81). SubLign leverages the longitudinal nature of patient data compared to the cross-sectional assumptions of PAGA (0.32) and SuStaIn (0.66). The Bayesian priors of [12] are likely too strong and may explain its poor performance (0.19). Dynamic time warping methods (0.06) perform poorly for few visits although results in the appendix show performance comparable to SubLign with a larger number of visits per patient. Lastly, the tensor factorization method [19] fails, likely because transforming data from continuous to discrete time results in a very large and extremely sparse matrix factorization and a tricky optimization problem. We specify the optimal parameters for the datasets and quadratic dataset experiments in the appendix.

**Parkinson’s disease dataset** SubLign recovers known subtypes in the PD dataset with higher ARI than baselines. SubLign identifies the two PD dataset subtypes with held-out ARI of  $0.585 \pm 0.128$  over five bootstrapped trials, compared to SubNoLign held-out ARI of  $0.423 \pm 0.143$  and KMeans+Loss held-out ARI of  $0.050 \pm 0.043$ .

**Visualization** The SubLign subtypes closely follow the true data generating functions (visualized in Figure 3). We plot the subtype by computing the latent space mean for all patients of each subtype, corresponding to Step 2 of Algorithm 1. In the appendix, the SubNoLign subtypes do not match as closely.

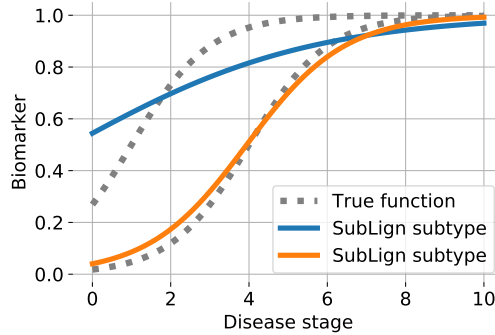


Figure 3: One of three biomarkers of learned SubLign subtypes from sigmoid data, plotted with original data generating function.

Table 2: Heart Failure SubLign subtypes (patient counts in parentheses) and statistically significant baseline feature means.

FEATURE	A (674)	B (444)	C (416)
Age	75.985	74.736	69.438
Female	0.712	0.234	0.435
Anemia	0.230	0.167	0.142
Atherosclerosis	0.285	0.349	0.401
Atrial Fibrillation	0.445	0.550	0.430
Chronic KD	0.277	0.349	0.341
Diastolic HF	0.504	0.363	0.067
Obese	0.568	0.653	0.462
Old MI	0.123	0.142	0.245
Pulmonary HD	0.295	0.225	0.190
Systolic HF	0.093	0.270	0.534

**Model misspecification** Our results are robust against reasonable model misspecification using piecewise polynomial data. Table 6 in the appendix shows 2 settings and 5 trials of SubLign learning on data generated from splines with 5 control points over 3 dimensions. Data size, dimensions, and noise rates are identical to synthetic datasets. In held-out ARI, SubLign outperforms SubNoLign and KMeans+Loss.

## 6.2 Recovering Known Alignment Values

For the sigmoid data, SubLign outperforms baselines in inferring alignment values (Table 1, Swaps and Pearson columns). Because it jointly models heterogeneity and alignment, SubLign recovers alignment values better according to the Swaps metric (mean value of 0.09) and the Pearson metric (mean value of 0.85) than the next best baselines of KMeans+Loss and SuStaIn. Note that some baselines only recover subtypes and do not learn patient alignment values.

In the HF semi-synthetic experiment, we find that SubLign is able to predict known alignment relationships. When evaluated on the manipulated test data, SubLign recovers the constructed relationship of  $\delta' > \delta''$  with a higher performance ( $71\% \pm 2\%$ ) over five trials compared to K-Means+Loss ( $57.8 \pm 4\%$ ) and SuStaIn ( $53.8 \pm 3\%$ ).

Table 3: Parkinson’s disease SubLign subtypes (patient counts in parentheses) and statistically significant baseline feature means.

MODEL	A (321)	B (298)
Healthy Control	0.551	0.064
Biological Dad With PD	0.028	0.068
Full Sibling With PD	0.010	0.058
UPSIT Part 1	7.558	5.493
UPSIT Part 2	7.648	5.695
UPSIT Part 3	6.988	5.238
UPSIT Part 4	7.539	5.624
UPSIT Total	29.732	22.050

### 6.3 Clinical insights from correcting for misalignment

We validate SubLign subtypes learned from the HF and PD datasets using known clinical findings. Tables 2 and 3 contain the mean of baseline features—not included as input to SubLign—that have statistically significant differences in means according to an analysis of variance with a Benjamini-Hochberg correction with a 0.05 false discovery rate: 8 features (out of 26) for PD and 15 features (out of 27) for HF. We include the full set of baseline features, including abbreviation explanations, in the appendix.

**Heart failure** SubLign recovers subtypes corresponding to—but not limited to—the two-group classification of HF patients based on ejection fraction: HF with reduced ejection fraction (systolic HF) and HF with preserved ejection fraction (diastolic HF). Despite this known dichotomy in cardiology, over 30% of patients in our dataset correspond to neither group. As a result, we set  $K = 3$ , one more than the number of currently known groups.

Although we lack ground truth subtype labels, we observe that SubLign finds 11 statistically significant baseline features (Table 2) including systolic HF and diastolic HF (two known subtypes of the disease). Subtype C corresponds to systolic HF, and subtype A and B correspond to diastolic HF, mirroring known clinical heterogeneity in diastolic HF [3]. Of the two subtypes corresponding to diastolic HF, subtype A has a higher proportion of women, and subtype B has a higher rate of obese patients; both subgroups with documented heterogeneity in diastolic HF [33, 34]. In contrast, the subtypes found by the KMeans+Loss baseline (Table 5 in appendix) have fewer statistically significant baseline features and do not include known subtypes—systolic HF and diastolic HF—as statistically significant features.

**Parkinson’s disease** SubLign discovers PD subtype features that match known clinical findings. This is important because biomarkers used to track PD are self-reported tests which can be biased, subjective, and noisy. We run SubLign with  $K = 2$  and present our results in Table 3 where we visualize the average values of baseline features stratified by the discovered subtypes. The differences in baseline features between the subtype corresponding to many healthy controls (subtype A) and subtype with fewer healthy controls (subtype B) closely match known clinical findings. The strongly statistically significant baselines include all components of the University of Pennsylvania Smell Identification Test (UPSIT) which is used in diagnosis. A lower UPSIT score demonstrates smell dysfunction, which is highly linked to PD [35]. Having a full sibling or biological dad with PD aligns with research that suggests PD may be partially hereditary [36].

## 7 Discussion

We study the task of clustering left-censored time-series data. After considering conditions for identifiability of subtype and alignment values, we present our method, SubLign, to learn latent representations of disease progression that correct for temporal misalignment in real-world observations. Empirically, our method outperforms eight baselines, and analysis of subtypes reveals clinically plausible findings. Better modeling of disease heterogeneity through alignment can help clinicians and scientists to better understand how chronic diseases with many subtypes may progress.

Our model introduces directions for future work. SubLign assumes that  $\delta$  and  $z$  are marginally independent. Intuitively, this condition means that, across all subtypes of a disease, the time at which the patient enters the data is independent of any other factor. There are certainly cases where this assumption may be violated, e.g., [37], which could be fertile ground for future work. We could also incorporate other complexities of clinical data, such as differences in treatment effect [38] or measurement biases within the healthcare system [39].

We hope that our model—in learning a continuous latent space to model heterogeneity—can be applied to other domains where subtypes and temporal alignment are entangled, for example gene expression analysis [40] or cancer pathways [41]. More broadly, this work contributes to making clinical models robust to real-world factors [42].

## 8 Acknowledgements

The authors thank Rebecca Boiarsky, Hunter Lang, and Monica Agrawal for helpful comments. Data used in the preparation of this article were obtained from the Parkinson’s Progression Markers Initiative (PPMI) database. PPMI — a public-private partnership — is funded by The Michael J. Fox Foundation for Parkinson’s Research and funding partners.

## References

- [1] Rupert G Miller Jr. *Survival analysis*, volume 66. John Wiley & Sons, 2011.
- [2] Finale Doshi-Velez, Yaorong Ge, and Isaac Kohane. Comorbidity clusters in autism spectrum disorders: An electronic health record time-series analysis. *Pediatrics*, 133(1), 2014.
- [3] Sanjiv J Shah, Daniel H Katz, Senthil Selvaraj, Michael A Burke, Clyde W Yancy, Mihai Gheorghiad, Robert O Bonow, Chiang-Ching Huang, and Rahul C Deo. Phenomapping for novel classification of heart failure with preserved ejection fraction. *Circulation*, 131(3):269–279, 2015.
- [4] Miriam S Udler, Jaegil Kim, Marcin von Grotthuss, Sílvia Bonás-Guarch, Joanne B Cole, Joshua Chiou, Christopher D. Anderson on behalf of METASTROKE, the ISGC, Michael Boehnke, Markku Laakso, Gil Atzmon, et al. Type 2 diabetes genetic loci informed by multi-trait associations point to disease mechanisms and subtypes: a soft clustering analysis. *PLoS medicine*, 15(9):e1002654, 2018.
- [5] Seyed-Mohammad Fereshtehnejad, Yashar Zeighami, Alain Dagher, and Ronald B Postuma. Clinical criteria for subtyping parkinson’s disease: biomarkers and longitudinal progression. *Brain*, 140(7):1959–1976, 2017.

- [6] Theophilus E Owan, David O Hodge, Regina M Herges, Steven J Jacobsen, Veronique L Roger, and Margaret M Redfield. Trends in prevalence and outcome of heart failure with preserved ejection fraction. *New England Journal of Medicine*, 355(3):251–259, 2006.
- [7] Leighton Chan, L Gary Hart, and David C Goodman. Geographic access to health care for rural medicare beneficiaries. *The Journal of Rural Health*, 22(2):140–146, 2006.
- [8] Sarah Miller and Laura R Wherry. Health and access to care during the first 2 years of the aca medicaid expansions. *New England Journal of Medicine*, 376(10):947–956, 2017.
- [9] Dwayne T Brandon, Lydia A Isaac, and Thomas A LaVeist. The legacy of tuskegee and trust in medical care: is tuskegee responsible for race differences in mistrust of medical care? *Journal of the National Medical Association*, 97(7):951, 2005.
- [10] KK Ho, Keaven M Anderson, William B Kannel, William Grossman, and Daniel Levy. Survival after the onset of congestive heart failure in framingham heart study subjects. *Circulation*, 88(1):107–115, 1993.
- [11] Alexandra L Young, Razvan V Marinescu, Neil P Oxtoby, Martina Bocchetta, Keir Yong, Nicholas C Firth, David M Cash, David L Thomas, Katrina M Dick, Jorge Cardoso, et al. Uncovering the heterogeneity and temporal complexity of neurodegenerative diseases with subtype and stage inference. *Nature communications*, 9(1):4273, 2018.
- [12] Ilkka Huopaniemi, Girish Nadkarni, Rajiv Nadukuru, Vaneet Lotay, Steve Ellis, Omri Gottesman, and Erwin P Bottinger. Disease progression subtype discovery from longitudinal emr data with a majority of missing values and unknown initial time points. In *AMIA Annual Symposium Proceedings*, volume 2014, page 709. American Medical Informatics Association, 2014.
- [13] Marwan A Mattar, Allen R Hanson, and Erik G Learned-Miller. Unsupervised joint alignment and clustering using bayesian nonparametrics. In *Proceedings of the Twenty-Eighth Conference on Uncertainty in Artificial Intelligence*, pages 584–593, 2012.
- [14] Scott J Gaffney and Padhraic Smyth. Joint probabilistic curve clustering and alignment. In *Advances in neural information processing systems*, pages 473–480, 2005.
- [15] Xiaoming Liu, Yan Tong, and Frederick W Wheeler. Simultaneous alignment and clustering for an image ensemble. In *2009 IEEE 12th International Conference on Computer Vision*, pages 1327–1334. IEEE, 2009.
- [16] Jennifer Listgarten, Radford M Neal, Sam T Roweis, Rachel Puckrin, and Sean Cutler. Bayesian detection of infrequent differences in sets of time series with shared structure. In *Advances in neural information processing systems*, pages 905–912, 2007.
- [17] Gang Li, Baosheng Liu, S Joe Qin, and Donghua Zhou. Dynamic latent variable modeling for statistical process monitoring. In *Proc. IFAC World Congress, Milan, Italy*, pages 12886–12891, 2011.
- [18] Yuan Luo, Alal Eran, Nathan Palmer, Paul Avillach, Ami Levy-Moonshine, Peter Szolovits, and Isaac S Kohane. A multidimensional precision medicine approach identifies an autism subtype characterized by dyslipidemia. *Nature Medicine*, 26(9):1375–1379, 2020.
- [19] Ioakeim Perros, Evangelos E Papalexakis, Fei Wang, Richard Vuduc, Elizabeth Searles, Michael Thompson, and Jimeng Sun. Spartan: Scalable parafac2 for large & sparse data. In *Proceedings of the 23rd ACM SIGKDD International Conference on Knowledge Discovery and Data Mining*, pages 375–384, 2017.

- [20] Ahmed M Alaa and Mihaela van der Schaar. Attentive state-space modeling of disease progression. In *Advances in Neural Information Processing Systems*, pages 11334–11344, 2019.
- [21] Diederik P Kingma and Max Welling. Auto-encoding variational bayes. *The 2nd International Conference on Learning Representations (ICLR)*, 2013.
- [22] Nat Dilokthanakul, Pedro AM Mediano, Marta Garnelo, Matthew CH Lee, Hugh Salimbeni, Kai Arulkumaran, and Murray Shanahan. Deep unsupervised clustering with gaussian mixture variational autoencoders. *arXiv preprint arXiv:1611.02648*, 2016.
- [23] Junyuan Xie, Ross Girshick, and Ali Farhadi. Unsupervised deep embedding for clustering analysis. In *International conference on machine learning*, pages 478–487, 2016.
- [24] Danilo Jimenez Rezende, Shakir Mohamed, and Daan Wierstra. Stochastic backpropagation and approximate inference in deep generative models. In *Proceedings of the 31st International Conference on International Conference on Machine Learning-Volume 32*, pages II–1278, 2014.
- [25] Adam Paszke, Sam Gross, Francisco Massa, Adam Lerer, James Bradbury, Gregory Chanan, Trevor Killeen, Zeming Lin, Natalia Gimelshein, Luca Antiga, et al. Pytorch: An imperative style, high-performance deep learning library. In *Advances in neural information processing systems*, pages 8026–8037, 2019.
- [26] Diederik P Kingma and Jimmy Ba. Adam: A method for stochastic optimization. *arXiv preprint arXiv:1412.6980*, 2014.
- [27] Xi Zhang, Jingyuan Chou, Jian Liang, Cao Xiao, Yize Zhao, Harini Sarva, Claire Henschcliffe, and Fei Wang. Data-driven subtyping of parkinson’s disease using longitudinal clinical records: a cohort study. *Scientific reports*, 9(1):1–12, 2019.
- [28] F Alexander Wolf, Fiona K Hamey, Mireya Plass, Jordi Solana, Joakim S Dahlin, Berthold Göttgens, Nikolaus Rajewsky, Lukas Simon, and Fabian J Theis. Paga: graph abstraction reconciles clustering with trajectory inference through a topology preserving map of single cells. *Genome biology*, 20(1):59, 2019.
- [29] Marco Cuturi. Fast global alignment kernels. In *Proceedings of the 28th international conference on machine learning (ICML-11)*, pages 929–936, 2011.
- [30] Marco Cuturi and Mathieu Blondel. Soft-dtw: a differentiable loss function for time-series. *arXiv preprint arXiv:1703.01541*, 2017.
- [31] Lawrence Hubert and Phipps Arabie. Comparing partitions. *Journal of classification*, 2(1):193–218, 1985.
- [32] Inderjit S Dhillon, Yuqiang Guan, and Brian Kulis. Kernel k-means: spectral clustering and normalized cuts. In *Proceedings of the tenth ACM SIGKDD international conference on Knowledge discovery and data mining*, pages 551–556, 2004.
- [33] Franz Duca, Caroline Zotter-Tufaro, Andreas A Kammerlander, Stefan Aschauer, Christina Binder, Julia Mascherbauer, and Diana Bonderman. Gender-related differences in heart failure with preserved ejection fraction. *Scientific reports*, 8(1):1–9, 2018.
- [34] Marijana Tadic and Cesare Cuspidi. Obesity and heart failure with preserved ejection fraction: a paradox or something else? *Heart Failure Reviews*, 24(3):379–385, 2019.

- [35] A Haehner, S Boesveldt, HW Berendse, A Mackay-Sim, J Fleischmann, PA Silburn, AN Johnston, GD Mellick, B Herting, H Reichmann, et al. Prevalence of smell loss in parkinson’s disease—a multicenter study. *Parkinsonism & related disorders*, 15(7):490–494, 2009.
- [36] Christine Klein and Ana Westenberger. Genetics of parkinson’s disease. *Cold Spring Harbor perspectives in medicine*, 2(1):a008888, 2012.
- [37] CC Kariyawasan, DA Hughes, MM Jayatillake, and AB Mehta. Multiple myeloma: causes and consequences of delay in diagnosis. *QJM: An International Journal of Medicine*, 100(10):635–640, 2007.
- [38] Susan Athey. Machine learning and causal inference for policy evaluation. In *Proceedings of the 21th ACM SIGKDD international conference on knowledge discovery and data mining*, pages 5–6, 2015.
- [39] Denis Agniel, Isaac S Kohane, and Griffin M Weber. Biases in electronic health record data due to processes within the healthcare system: retrospective observational study. *Bmj*, 361:k1479, 2018.
- [40] Ziv Bar-Joseph, Georg Gerber, David K Gifford, Tommi S Jaakkola, and Itamar Simon. A new approach to analyzing gene expression time series data. In *Proceedings of the sixth annual international conference on Computational biology*, pages 39–48, 2002.
- [41] Hao Wu, Lin Gao, and Nikola Kasabov. Inference of cancer progression from somatic mutation data. *IFAC-PapersOnLine*, 48(28):234–238, 2015.
- [42] Marzyeh Ghassemi, Tristan Naumann, Peter Schulam, Andrew L Beam, Irene Y Chen, and Rajesh Ranganath. Practical guidance on artificial intelligence for health-care data. *The Lancet Digital Health*, 1(4):e157–e159, 2019.



# Appendix

We present appendix for our submission, entitled “Clustering Censored Multivariate Time-Series for Disease Phenotyping.”

- In Section A, we detail the experiment setup details and additional results for sigmoid experiments. We also detail experiment setup details for clinical experiments.
- In Section B, we present the proof for conditions of identifiability.
- In Section C, we detail the quadratic experiments setup, optimal parameters, and results.
- In Section D, we present an additional baseline table from the heart failure clinical experiments.

## A Experiment setup details

Here we describe additional details about experiment setup:

- In Section A.1, we describe the swaps metric.
- In Section A.2, we describe the specific parameters used for the baselines.
- In Section A.3, we specify the optimal hyperparameters chosen for sigmoid experiments and clinical experiments.
- In Section A.4, we plot SubNoLign subtypes for sigmoid data.
- In Section A.5, we detail the biomarkers and baseline features used for both clinical datasets: heart failure and Parkinson’s disease.
- In Section A.6, we describe how SubLign handles missing values, including irregularly lengths of time-series data.

### A.1 Swaps Metric

For true sorted alignment values  $a_1, \dots, a_N$  for  $N$  patients, we define the swaps metric  $\mathcal{S}$  of proposed alignment values  $b_1, \dots, b_N$  as the number of swaps needed to sort the predicted disease times into the true disease stages, expressed as percentage of total possible swaps.

$$\mathcal{S} = \frac{\sum_{i,j;i < j} \mathbb{1}(a_i < b_i, a_j > b_j)}{N(N-1)/2}$$

### A.2 Baselines

We outline SubNoLign and KMeans+Loss in the main paper. Here we describe the remaining baselines.

**SuStaIn** SuStaIn [11] is a disease progression algorithm that recovers subtype and stage from cross-sectional data. We transform our longitudinal data by dropping patient affiliation across visits. We transform the data by subtracting the mean for each feature and dividing by the standard deviation for each feature. We assume the Z-scored values have a max of 5. We run for 1,000,000 epochs for the Markov Chain Monte Carlo sampling and 1,000 epochs for optimization. We use an open source implementation by the authors.<sup>1</sup>

---

<sup>1</sup><https://github.com/ucl-pond/pySuStaIn>

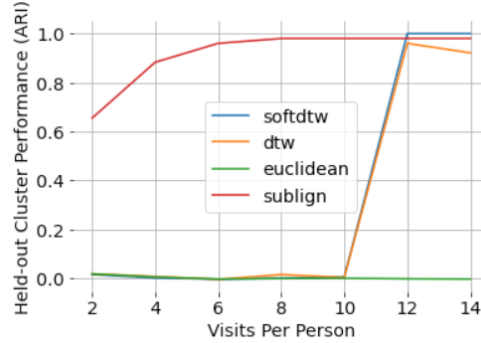


Figure 4: Cluster performance (ARI) on held-out data for baseline methods of time series K-means with different distance functions. DTW methods match SubLign performance on larger number of visits per patient.

**Bayesian approach** The Bayesian approach [12] assumes longitudinal data, but there must be a small number of measured time points. We assume that there are 10 observed time points where observed data can begin as well as a window of 10 time points before the observed window where a patient’s values can be aligned to. Because biomarker values are scaled between 0 and 10, we assume that values change between time points based on a Gaussian with  $\sigma = 2$  and that subtype means for each time point are drawn from a Gaussian with  $\sigma = 5$ . We draw 4000 samples and use the maximum a posteriori estimate to determine stage and subtype for test patients. Because we could not find an open-source option, we implemented the algorithm ourselves based on the description in the paper.

**PAGA** Partition-based graph abstraction, or PAGA, [28] assumes cross-sectional data, so we create separate visits for each patient visit. For algorithm parameters, we set resolution to 0.05, number of neighbors to 15, and connectivity cutoff of 0.05. We use an open source implementation by the authors.<sup>2</sup>

**Dynamic time warping** Dynamic time warping (DTW) defines similarity between time series that can be combined with clustering techniques. DTW methods include using soft-DTW [30] and kernel [29] before using K-means with the chosen similarity metric. We use open source implementations of DTW algorithms<sup>3</sup> to generate our baseline comparisons. Although DTW methods perform poorly against SubLign, held-out performance of DTW methods can match SubLign performance on larger number of visits per patient (Figure 4).

**Tensor factorization** Sparse tensor factorization has been used for disease phenotyping. The decomposition of large and sparse datasets using canonical polyadic decomposition can create an interpretable output for phenotyping. We use the Matlab open source implementation of SPARTan.<sup>4</sup> We found these baseline results to yield poor clustering performance despite aggressive hyperparameter tuning. We surmise this is because transforming our data from continuous to discrete time resulted in a very large and extremely sparse matrix factorizing which is a tricky optimization problem.

<sup>2</sup>[https://github.com/dynverse/ti\\_paga/blob/master/run.py](https://github.com/dynverse/ti_paga/blob/master/run.py)

<sup>3</sup><https://pypi.org/project/dtw-python/>

<sup>4</sup><https://github.com/kperros/SPARTan>

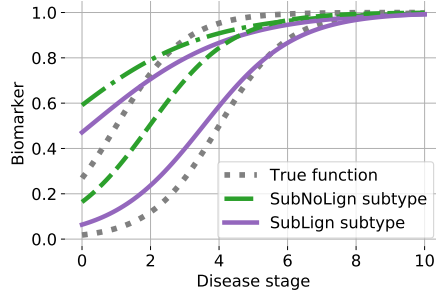


Figure 5: One of three dimensions of learned SubLign and SubNoLign subtypes from sigmoid synthetic data plotted on top of original data generating functions.

### A.3 Optimal hyperparameters for sigmoid and clinical baselines

For the sigmoid dataset, the optimal hyperparameters are latent space of dimension 5, 100 hidden units in the RNN, 50 hidden units in the multi-layer perceptron, learning rate of 0.01, and no regularization.

For the Parkinson’s disease dataset, we searched on a slightly smaller set of hyperparameters for SubLign and found optimal hyperparameters of  $\beta = 0.01$ , no regularization, 10 latent dimensions, 10 hidden units for the multi-layer perceptron, 200 units for the recurrent neural network, and learning rate of 0.1.

For the heart failure dataset, we searched on a slightly smaller set of hyperparameters for SubLign and found optimal hyperparameters of  $\beta = 0.001$ , no regularization, 10 latent dimensions, 20 hidden units for the multi-layer perceptron, 50 units for the recurrent neural network, and learning rate of 0.01.

### A.4 SubNoLign subtype visualization

We find that the visualization of the SubNoLign subtypes are not as close to the data generating function as the SubLign subtypes for the sigmoid dataset in Figure 5. All other parameters, data dimensions, and experimental conditions are held constant.

### A.5 Clinical dataset biomarkers and baseline features

For the heart failure dataset, we include the following biomarkers: Aorta - Ascending, Aorta - Valve Level, Aortic Valve - Peak Velocity, Left Atrium - Four Chamber Length, Left Atrium - Long Axis Dimension, Left Ventricle - Diastolic Dimension, Left Ventricle - Ejection Fraction, Left Ventricle - Inferolateral Thickness, Left Ventricle - Septal Wall Thickness, Mitral Valve - E Wave, Mitral Valve - E Wave Deceleration Time, and Right Atrium - Four Chamber Length.

From the Parkinson’s Progression Markers Initiative (PPMI) dataset, we include four main biomarkers: 1) MOCA, a cognitive assessment, 2) SCOPA-AUT, an autonomic assessment, 3) NUPDRS1, an assessment of non-motor symptoms, and 4) a maximum taken over NUPDRS3 and NUPDRS2 as an assessment of motor symptoms.

The baseline features considered for heart failure are: age, anemia, atherosclerosis, atrial fibrillation, Black, body mass index, chronic kidney disease, diastolic heart failure, esophageal reflux, female, hyperlipidemia, hypertension, hypothyroidism, kidney disease, major depressive disorder, obesity old myocardial infarction, other race, pulmonary heart disease, pneumonia, renal failure, type 2 diabetes, urinary tract infection, and White.

---

**Algorithm 2** Procedure for the identification of model parameters

---

- 1: **Input:** Visit times  $X \in \mathbb{R}^{N \times M}$ , biomarkers  $Y \in \mathbb{R}^{N \times M \times D}$ , polynomial degree  $P$ , invertible function  $f$
  - 2: **Output:**  $\theta^P, \delta_1, \dots, \delta_N, s_1, \dots, s_N$  for each patient
  - 3: **Step 1: Transform the observed biomarkers;**  $Q = f^{-1}(Y)$
  - 4: **Step 2: Obtain time-shifts using a single biomarker;**
  - 5: a) For each patient  $i$ , estimate the parameters  $\theta^1_i$  of  $\kappa(x; \theta^1_i)$  using a single biomarker  $((x_{i,1}, q_{i,1}), \dots, (x_{i,M}, q_{i,M}))$  via polynomial regression,
  - 6: b) Compute up to  $P$  roots of polynomial  $\kappa(x, \theta^1_i)$  for each patient  $i$  as  $R_i = \{r_1, \dots, r_P\}$  and set  $\xi_i = \min \text{Real}(R_i)$  where Real denotes the real part of (potentially complex) roots.
  - 7: c) Estimate  $\tilde{\theta}^1_i$  for polynomials in a *canonical position* using  $((x_{i,1} - \xi_i, q_{i,1}), \dots, (x_{i,M} - \xi_i, q_{i,M}))$  via polynomial regression,
  - 8: d) Cluster  $\tilde{\theta}^j_i$  across patients via K-means clustering to yield cluster identities  $s_1, \dots, s_N$
  - 9: e)  $\forall k, \eta_k = \min\{\xi_i \mid i \text{ s.t. } s_i = k\}$  and  $\forall i, \delta_i = \xi_i - \eta_{s_i}$
  - 10: **Step 3: Estimate true polynomial coefficients using shifted observation times;**
  - 11: **for** biomarker  $j = 1$  **to**  $J$  **do**
  - 12:   For each patient, estimate the parameters  $\theta^j_i$  of  $\kappa(x; \theta^j_i)$  using  $((x_{1,1} - \delta_i, q_{1,1}[j]), \dots, (x_{1,M} - \delta_i, q_{1,M}[j]))$  via polynomial regression,
  - 13: **end for**
  - 14: Return  $\theta^P = [\theta^1 \mid \dots \mid \theta^J], \{\delta_1, \dots, \delta_N\}, \{s_1, \dots, s_N\}$
- 

The baseline features considered for Parkinson’s disease (PD) are: male, Hispanic/Latino, White, Asian, Black, American Indian, Pacific Islander, not specified race, biological mom with PD, biological dad with PD, full sibling with PD, half sibling with PD, maternal grandparent with PD, paternal grandparent with PD, maternal aunt/uncle with PD, paternal aunt/uncle with PD, kids with PD, years of education, right handed, left handed, University of Pennsylvania Smell Identification Test (UPSIT) part 1, UPSIT part 2, UPSIT part 3, UPSIT part 4, and UPSIT total.

## A.6 Missing values

SubLign allows for missing biomarker dimensions and missing patient visits to accommodate the sparsity of clinical data. For the recognition network input, we linearly interpolate missing values for each patient. For missing visits, we adapt the decoder to handle variable sequence lengths. We mask out missing values and visits so they have no contribution to the learning stage. For patients with no measurements of a biomarker, we mean-interpolate from values from all other patients.

## B Identifiability

We restate our assumptions.

**Assumption 1.**  $f$  is invertible, and  $\kappa(x, \theta) = \theta_0 + \sum_{p=1}^P \theta_p x^p$  describes a family of polynomial functions in  $x$  with parameter  $\theta$  and degree  $P > 0$ . The parameters of each subtype are unique.

**Assumption 2.**  $M \geq P + 1$ , i.e., for each object, across all the  $J$  features, we observe at least  $P + 1$  values.

**Assumption 3.** For each subtype  $s_k$ , there exists an object  $i$  whose alignment  $\delta_i = 0$ .

We provide the proof for Theorem 1 below:

*Proof.* The proof is constructive; i.e. we give an algorithm for the identification of the parameters of the model in Equation 2. The algorithm for identification is presented in Algorithm 2 and proceeds in three steps.

**Step 1:** The first step transforms the observed biomarkers by applying the inverse of function  $f$ , which exists by Assumption 1. This leaves us with data as:

$$f^{-1}(y_{i,m}) = \kappa(x_{i,m} + \delta_i; \theta_{s_i}^P) \quad \forall i \in N, m \in M$$

i.e. for all bio-markers, across all patients, we have data arising from different polynomial functions.

**Step 2:** Without loss of generality, the second step uses the first biomarker to identify the values of  $\delta_i$  for each patient.

- a) First, we estimate the polynomial coefficients for each patient separately; we are guaranteed exact recovery of the coefficients by Assumption 2.
- b) Next we find the roots for each polynomial. If they are complex, consider their real part, and define  $\xi_i$  to be the smallest root of the polynomial. At least one (real or complex) root is guaranteed to exist by the Fundamental Theorem of Algebra for every non-constant polynomial (Assumption 1). Note that the choice of using the smallest root is arbitrary; what matters is that a consistent choice of root is selected for each patient's polynomials.
- c) The goal of this step to learn a new polynomial for each patient which is translated to ensure that the root selected in step b) lies at  $x = 0$ .

To do so, we first shift the observational time-steps by  $\xi_i$ , and we re-estimate the coefficients of each *shifted* polynomial.

We make use of the fact that if  $\xi_i$  is the smallest complex root of a polynomial  $\kappa(x)$  then the polynomial  $\kappa(x + \xi_i)$  has its smallest complex root at 0. We can recover the parameters of this polynomial exactly by shifting our observations and re-estimating the coefficients.

This operation recovers the coefficients of every patient's polynomial in its *canonical position* i.e. a translated polynomial whose the smallest root (or its real component) is at  $x = 0$ .

This step can be viewed as a de-biasing step which allows us to re-estimate  $\tilde{\theta}$  without while ignoring the effect that left-censorship has on parameter estimates.

- d) We cluster the coefficients estimated in step c). By construction, we know that  $s_i = s_{i'} \iff \theta_i = \theta_{i'}$  which guarantees that clustering recovers the true-underlying subtype for each patient (up to a permutation over  $K$  choices).
- e) Finally we stratify patients by their subtype, and we define  $\delta_i$  as the difference between their smallest root and the smallest value of  $\xi_i$  among all other patients within that subtype.

By Assumption 3, we know that for each subtype, there exists a patient for whom  $\delta_i = 0$ , this reference patient will also be the one whose polynomial has the smallest root. We note here that without Assumption 3, we would still have identification of  $\delta_i$  up to a constant.

Therefore, by shifting each patient's smallest root by their reference patient's smallest root, we can recover the original time-shifts.

**Step 3:** Given the values of  $\delta_1, \dots, \delta_N$  from Step 2, we can now estimate the true values of the polynomial coefficients exactly in the noiseless setting via polynomial regression.  $\square$

## C Quadratic experiments

We describe an additional set of experiments using the quadratic functional family. These experiments were designed to better understand where SubLign is able to learn clustering and alignment metrics well.

- In Section C.1, we detail the dataset creation.
- In Section C.2, we outline the optimal hyperparameters for the quadratic experiments.
- In Section C.3, we describe the empirical results against known baselines.

### C.1 Setup

For the quadratic dataset, we generate data from 2 subtypes and 1 dimension with generating functions. See Table 4 for subtype generating functions. Similar to the sigmoid synthetic dataset, for each patient in the datasets, we draw subtype  $\kappa \sim \text{Bern}(0.5)$ . The true disease stage is drawn  $t_m \sim U(0, T^+)$  for visit  $m \in [M]$ . The biomarker values are drawn  $y_m \sim N(\mu_m, S)$  where  $\mu_m = \sum_{k \in [K]} \mathbb{1}(\kappa = k) f_k(t_m)$ . The observed disease time  $x_m$  is shifted such that the first patient visit is at time 0. Therefore  $x_m = t_m - \tau$  where  $\tau = \min_{j \in [M]} t_j$  and is the earliest true disease time for the patient. We sample  $N = 1000$  patients with  $M = 4$  patient visits with noise  $S = 0.25$  and upper time bound  $T^+ = 10$ .

FIGURE	DESCRIPTION	SUBTYPE GENERATING FUNCTIONS
6	Quadratic curve and flat line, separable	$f_1(t) = 0.25t^2 - 2.2t + 5,$ $f_2(t) = 2$
7	Quadratic curve and flat line, overlapping	$f_1(t) = 0.25t^2 - 2.2t + 5,$ $f_2(t) = -2$
8	Quadratic curve and sloped line, separable	$f_1(t) = 0.25t^2 - 2.2t + 5,$ $f_2(t) = 0.4t$
9	Quadratic curve and sloped line, overlapping	$f_1(t) = 0.25t^2 - 2.2t + 5,$ $f_2(t) = 0.4t - 5$
10	Quadratic curves in opposite directions, separable	$f_1(t) = 0.25t^2 - 2.2t + 3,$ $f_2(t) = -0.25t^2 + 2.2 - 5$
11	Quadratic curves in opposite directions, overlapping	$f_1(t) = 0.25t^2 - 2.2t + 7,$ $f_2(t) = -0.25t^2 + 2.2 - 5$

Table 4: Quadratic dataset subtype generating functions and corresponding figure numbers

We construct our quadratic experiments such that we examine different model classes (i.e. flat, linear, quadratic) as well as examine subtypes that are overlapping or separable.

We include baseline results for the quadratic datasets. Note that SuStaIn [11] assumes monotonically increasing functions and is therefore omitted. We denote degenerate solutions with dashes.

## C.2 Optimal hyperparameters for quadratic datasets

For the synthetic quadratic dataset corresponding to Figure 6, we found the optimal hyperparameters for SubLign as no regularization, 5 hidden dimensions for the multi-layer perceptron, 200 latent dimensions, 200 units for the recurrent neural network, and learning rate of 0.001.

For the synthetic quadratic dataset corresponding to Figure 7, we found the optimal hyperparameters for SubLign as no regularization, 5 hidden dimensions for the multi-layer perceptron, 200 latent dimensions, 200 units for the recurrent neural network, and learning rate of 0.001.

For the synthetic quadratic dataset corresponding to Figure 8, we found the optimal hyperparameters for SubLign as no regularization, 5 hidden dimensions for the multi-layer perceptron, 200 latent dimensions, 200 units for the recurrent neural network, and learning rate of 0.001.

For the synthetic quadratic dataset corresponding to Figure 9, we found the optimal hyperparameters for SubLign as no regularization, 5 hidden dimensions for the multi-layer perceptron, 200 latent dimensions, 200 units for the recurrent neural network, and learning rate of 0.001.

For the synthetic quadratic dataset corresponding to Figure 10, we found the optimal hyperparameters for SubLign as no regularization, 5 hidden dimensions for the multi-layer perceptron, 200 latent dimensions, 200 units for the recurrent neural network, and learning rate of 0.001.

For the synthetic quadratic dataset corresponding to Figure 10, the optimal hyperparameters are latent space of dimension 10, 20 hidden units in the RNN, 50 hidden units in the multi-layer perceptron, learning rate of 0.01, and no regularization.

For the synthetic quadratic dataset corresponding to Figure 11, the optimal hyperparameters are latent space of dimension 5, 100 hidden units in the RNN, 50 hidden units in the multi-layer perceptron, learning rate of 0.01, and no regularization.

## C.3 Results

In Figures 6 to 11, we present the quantitative results of 6 different quadratic cases as well as a plot of example data and the data generating subtypes. In each, we see that SubLign or SubNoLign outperforms the baselines.

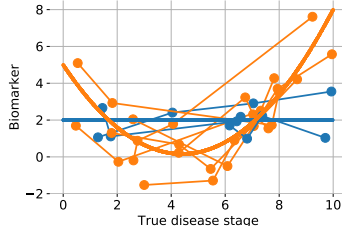
When the subtypes are separable (i.e. Fig 7, 9, and 11), SubLign handily recovers the subtypes. When the subtypes are not separable (i.e. Fig 6, 8, and 10), SubLign still outperforms baselines.

We note that alignment metrics are especially challenging to recover when one subtype is a flat or sloped line as in with Figure 6 to 11. Because the alignment metric is entirely unidentifiable, the swaps and Pearson metrics suffer. Note that for the swaps metric, 0.5 corresponds to random guessing, so the lack of identifiability of one of the subtypes would cause a swaps metric of 0.25. When the second subtype has a changing slope, as in Figure 10, the alignment metrics are more recoverable.

When the model is degenerate and does not return the alignment values, we denote this with an empty cell.

## D Heart Failure Baseline Experiment

We present the KMeans+Loss subtypes on the heart failure dataset (Table 2).



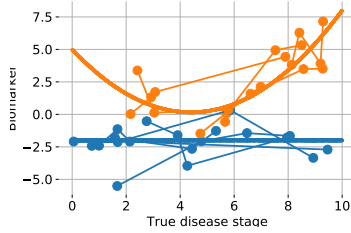
MODEL	ARI $\uparrow$	SWAPS $\downarrow$	PEARSON $\uparrow$
SubLign	$0.277 \pm 0.040$	$0.277 \pm 0.014$	$0.516 \pm 0.007$
SubNoLign	$0.103 \pm 0.002$	—	—
KMeans+Loss	$0.213 \pm 0.009$	$0.498 \pm 0.022$	$0.016 \pm 0.051$
SuStaIn [11]	0.151	0.203	0.000
Bayesian [12]	$0.000 \pm 0.000$	$0.501 \pm 0.017$	$0.018 \pm 0.125$
PAGA [28]	$0.027 \pm 0.001$	—	—

Figure 6: Synthetic results over 5 trials. **Top:** Data generating functions for two subtypes (thick lines) and example aligned patients (dots and thin lines). **Bottom:** SubLign outperforms baselines while KMeans+Loss recovers subtypes (ARI metric) better than SubNoLign, but alignment metrics are difficult to recover because of the horizontal subtype

FEATURE	A (240)	B (802)	C (492)
Age	71.567	74.565	73.793
Hyperlipidemia	0.529	0.448	0.541
Chronic KD	0.346	0.273	0.370
Esophageal Reflux	0.375	0.259	0.289
Pulmonary Heart Disease	0.367	0.204	0.256
Kidney Disease	0.254	0.200	0.278
Atherosclerosis	0.196	0.131	0.201
Anemia	0.217	0.163	0.213
Obese	0.688	0.500	0.608

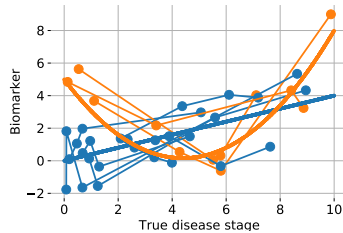
Table 5: Heart Failure KMeans+Loss subtypes (patient counts in parentheses), described by mean baseline features. Only statistically significant features are listed and do not include systolic and diastolic HF, two known phenotypes of HF.





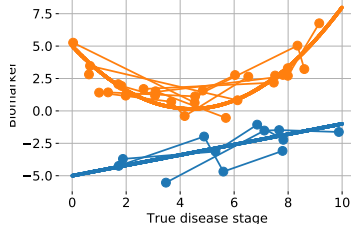
MODEL	ARI $\uparrow$	SWAPS $\downarrow$	PEARSON $\uparrow$
SubLign	$0.980 \pm 0.000$	$0.253 \pm 0.001$	$0.527 \pm 0.011$
SubNoLign	$0.980 \pm 0.000$	—	—
KMeans+Loss	$0.883 \pm 0.000$	$0.471 \pm 0.011$	$0.064 \pm 0.067$
SuStaIn [11]	$0.228 \pm 0.039$	$0.182 \pm 0.010$	$0.000 \pm 0.000$
Bayesian [12]	$0.198 \pm 0.189$	$0.446 \pm 0.052$	$0.157 \pm 0.286$
PAGA [28]	$0.227 \pm 0.035$	—	—

Figure 7: Synthetic results over 5 trials. **Top:** Data generating functions for two subtypes (thick lines) and example aligned patients (dots and thin lines). **Bottom:** SubLign and SubNoLign have near-perfect clustering accuracy (ARI) while alignment metrics (swaps, Pearson) are difficult recover because of the horizontal subtype.



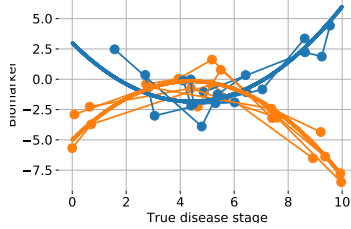
MODEL	ARI $\uparrow$	SWAPS $\downarrow$	PEARSON $\uparrow$
SubLign	$0.122 \pm 0.006$	$0.272 \pm 0.001$	$0.621 \pm 0.020$
SubNoLign	$0.145 \pm 0.006$	—	—
KMeans+Loss	$0.031 \pm 0.030$	$0.302 \pm 0.026$	$0.498 \pm 0.010$
SuStaIn [11]	$0.138 \pm 0.019$	$0.119 \pm 0.006$	$0.000 \pm 0.000$
Bayesian [12]	$0.001 \pm 0.002$	—	—
PAGA [28]	$0.009 \pm 0.000$	—	—

Figure 8: Synthetic results over 5 trials. **Top:** Data generating functions for two subtypes (thick lines) and example aligned patients (dots and thin lines). **Bottom:** SubLign outperforms baselines in clustering and alignment metrics although the task is challenging.



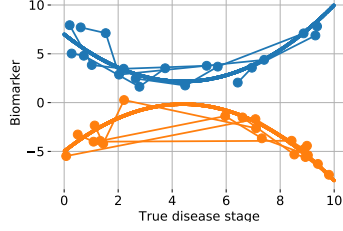
MODEL	ARI $\uparrow$	SWAPS $\downarrow$	PEARSON $\uparrow$
SubLign	$0.968 \pm 0.016$	$0.253 \pm 0.015$	$0.604 \pm 0.041$
SubNoLign	$0.968 \pm 0.016$	—	—
KMeans+Loss	$0.964 \pm 0.008$	$0.486 \pm 0.032$	$0.044 \pm 0.101$
SuStaIn [11]	$0.220 \pm 0.011$	$0.196 \pm 0.008$	$0.000 \pm 0.000$
Bayesian [12]	$0.221 \pm 0.214$	$0.448 \pm 0.070$	$0.165 \pm 0.193$
PAGA [28]	$0.205 \pm 0.012$	—	—

Figure 9: Synthetic results over 5 trials. **Top:** Data generating functions for two subtypes (thick lines) and example aligned patients (dots and thin lines). **Bottom:** SubLign, SubNoLign, and KMeans+Loss perform well on clustering.



MODEL	ARI $\uparrow$	SWAPS $\downarrow$	PEARSON $\uparrow$
SubLign	$0.729 \pm 0.049$	$0.153 \pm 0.006$	$0.843 \pm 0.016$
SubNoLign	$0.721 \pm 0.035$	—	—
KMeans+Loss	$0.540 \pm 0.034$	$0.490 \pm 0.020$	$0.043 \pm 0.057$
SuStaIn [11]	$0.198 \pm 0.024$	$0.200 \pm 0.008$	$0.000 \pm 0.000$
Bayesian [12]	$0.003 \pm 0.007$	—	—
PAGA [28]	$0.059 \pm 0.006$	—	—

Figure 10: Synthetic results over 5 trials. **Top:** Data generating functions for two subtypes (thick lines) and example aligned patients (dots and thin lines). **Bottom:** SubLign learns subtypes and recovers alignment better than baselines.



MODEL	ARI $\uparrow$	SWAPS $\downarrow$	PEARSON $\uparrow$
SubLign	$1.000 \pm 0.000$	$0.134 \pm 0.012$	$0.907 \pm 0.009$
SubNoLign	$0.984 \pm 0.008$	—	—
KMeans+Loss	$1.000 \pm 0.000$	$0.508 \pm 0.034$	$0.014 \pm 0.095$
SuStaIn [11]	$0.148 \pm 0.032$	$0.247 \pm 0.016$	$0.000 \pm 0.000$
Bayesian [12]	$0.261 \pm 0.349$	$0.409 \pm 0.052$	$0.303 \pm 0.119$
PAGA [28]	$0.233 \pm 0.017$	—	—

Figure 11: Synthetic results over 5 trials. **Top:** Data generating functions for two subtypes (thick lines) and example aligned patients (dots and thin lines). **Bottom:** SubLign learns subtypes and alignment values.

MODEL	ARI $\uparrow$	PEARSON $\uparrow$	SWAPS $\downarrow$
SubLign-Incr	$0.82 \pm 0.17$	$0.83 \pm 0.08$	$0.14 \pm 0.04$
SubNoLign-Incr	$0.77 \pm 0.10$	—	—
KMeans+Loss-Incr	$0.58 \pm 0.11$	$0.43 \pm 0.09$	$0.21 \pm 0.06$
SubLign-Any	$0.46 \pm 0.12$	$0.67 \pm 0.39$	$0.22 \pm 0.14$
SubNoLign-Any	$0.29 \pm 0.10$	—	—
KMeans+Loss-Any	$0.22 \pm 0.07$	$0.23 \pm 0.21$	$0.48 \pm 0.11$

Table 6: Model misspecification experiment means and standard deviations using 5 cubic splines datasets.